

# Controlled Synthesis and Photoluminescence Properties of ZnS Nanowires and Nanoribbons

Soumitra Kar and Subhadra Chaudhuri\*

Department of Materials Science, Indian Association for the Cultivation of Science,  
Jadavpur, Kolkata 700 032, India

Received: September 15, 2004; In Final Form: December 7, 2004

Rapid synthesis of wurtzite ZnS nanowires and nanoribbons has been achieved by a simple thermal evaporation of ZnS powder onto Si substrate in the presence of Au catalyst. A vapor–liquid–solid process is proposed for the formation of the ZnS nanostructures. The flow rate of the inert carrier Ar gas along with the temperature play an important role in defining the morphology of the ZnS nanostructures. The morphological change of the ZnS nanostructures and their growth sequence were studied through scanning electron microscopy. Room-temperature photoluminescence measurements showed intense blue emission at  $\sim 398$  nm from both the nanowires and the nanoribbons.

## Introduction

Zinc sulfide, an important semiconductor compound of the IIB–VI groups, has a wide band-gap energy of  $3.7\text{ eV}^1$  at 300 K. ZnS is a luminescent material well known for its photoluminescence,<sup>2</sup> electroluminescence,<sup>3</sup> etc., which enable wide applications in the fields of displays,<sup>4</sup> sensors, and lasers.<sup>2,5</sup> Moreover, zinc sulfide is also widely used in photocatalysis.<sup>6,7</sup> In recent years, nanocrystalline ZnS attracted much attention because properties in nanoforms differ significantly from those of their bulk counterparts.<sup>8</sup> Therefore, much effort has been made to control the size, morphology, and crystallinity of the ZnS nanocrystals with a view to tune their physical properties. The recent trend in nanomaterials research is toward one-dimensional nanostructured materials because of their wide range of potential applications in nanoscale devices.<sup>9–12</sup> One-dimensional ZnS nanostructures such as nanorods,<sup>13</sup> nanowires,<sup>14,15</sup> nanobelts,<sup>16–18</sup> and nanotubes<sup>19</sup> have been produced by different synthesis techniques such as the solvothermal process,<sup>13</sup> thermal evaporation of ZnS powder,<sup>14–18</sup> liquid crystal template method,<sup>20</sup> etc.

Meng et al.<sup>15</sup> have produced sphalerite (cubic) ZnS nanowires by hydrogen-assisted thermal evaporation of ZnS powder at  $1100\text{ }^\circ\text{C}$  for 3 h onto a Au-coated Si substrate placed 30 cm away from the source. Wurtzite ZnS nanowires were synthesized by Wang et al.<sup>14</sup> by thermal evaporation of ZnS powder at  $900\text{ }^\circ\text{C}$  for 2 h onto the Au-coated Si wafer. Li et al.<sup>16</sup> have reported wurtzite ZnS nanobelts synthesized by thermal evaporation of ZnS powder at  $1200\text{ }^\circ\text{C}$  for 2 h. Two groups have reported hydrogen-assisted growth of ZnS nanostructures<sup>17,18</sup> by thermal evaporation of ZnS powder at temperature over  $1100\text{ }^\circ\text{C}$  for a time period of 1.5–4 h. All of the above fabrication processes of the ZnS nanowires and nanobelts were time-consuming. In addition, the effect of the flow rate of the carrier Ar gas in defining the morphology of the one-dimensional nanostructures has not been studied so far.

In this paper, we report rapid (30 min) production and morphological control of wurtzite nanostructures on a large scale by thermal evaporation of ZnS powder on Si wafer coated with a thin layer of Au ( $\sim 25\text{ \AA}$ ). The role of the flow rate of carrier Ar gas in determining the morphology of the ZnS nanostructures

has been established. Photoluminescence properties of these ZnS nanowires and nanoribbons are also reported.

## Experimental Section

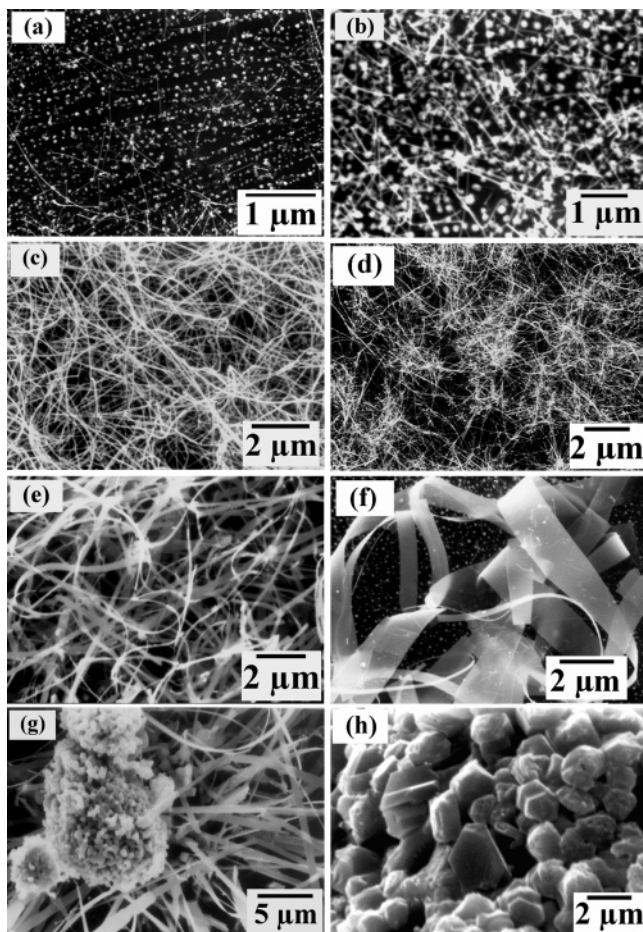
A conventional horizontal tube furnace was used for the synthesis. The experimental setup consisted of a one-end open quartz tube fitted with a rotary vacuum pump and an Ar gas inlet through a vacuum coupling. Si wafers used, as the substrates, were first ultrasonically cleaned in acetone for 20 min and then sputter coated with a thin ( $\sim 25\text{ \AA}$ ) layer of Au film. Analytical grade ZnS powder was loaded in a quartz boat, and the Au-coated Si wafer was clipped over the boat. The vertical distance between the ZnS powder and the Si substrate was maintained at 3 mm. The quartz boat was then placed near the closed end of the quartz tube, and, after the quartz tube was evacuated, Ar gas was flowed through it during the entire deposition period. The quartz tube was then inserted into the preheated tube furnace, and, after 30 min of deposition, it was taken out of the furnace to allow rapid cooling to room temperature. The deposition temperature and the flow rate of the Ar gas were varied within a certain range.

The products were characterized using an X-ray diffractometer (XRD, Seifert 3000P) with Cu K $\alpha$  radiation, and the compositional analysis was done by energy-dispersive analysis of X-ray (EDAX, Kevex, Delta Class I). Microstructures of the nanoforms were obtained by scanning electron microscopy (SEM, Hitachi S-3200) and transmission electron microscopy (TEM, JEM 3000F). The high-resolution transmission electron microscopic (HRTEM) image and the typical selected area electron diffraction (SAED) pattern of ZnS nanowire and nanoribbons were also taken. Photoluminescence (PL) measurements were carried out at room temperature using 250 nm as the excitation wavelength with a luminescence spectrometer (Perkin-Elmer, LS50B).

## Results and Discussion

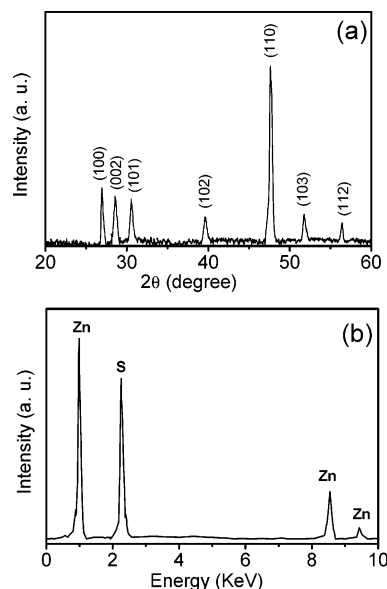
**Morphology of the ZnS Nanostructures.** The morphology of the ZnS nanostructures investigated through SEM was found to be highly influenced by the experimental parameters such as temperature and flow rate of the Ar gas. With a view to investigate the role of these parameters in defining the morphology of the products, we have performed the synthesis at four

\* Corresponding author. Tel.: +91-033-2473-4971. Fax: +91-033-2473-2805. E-mail: mssc2@mahendra.iacs.res.in.



**Figure 1.** SEM images showing different morphologies of ZnS nanostructures produced with different sets of temperatures and Ar gas flow rates: (a) 850 °C and 100 cm<sup>3</sup>/min, (b) 850 °C and 800 cm<sup>3</sup>/min, (c) 950 °C and 100 cm<sup>3</sup>/min, (d) 950 °C and 800 cm<sup>3</sup>/min, (e) 1050 °C and 100 cm<sup>3</sup>/min, (f) 1050 °C and 800 cm<sup>3</sup>/min, (g) 1150 °C and 100 cm<sup>3</sup>/min, and (h) 1150 °C and 800 cm<sup>3</sup>/min.

different temperatures (850, 950, 1050, and 1150 °C) along with two different flow rates (100 and 800 cm<sup>3</sup>/min) for each temperature. For the SEM observation, the as-deposited Si wafers were directly transferred to the SEM chamber without distorting the original nature of the products. Figure 1a shows the product obtained at 850 °C with a lower flow rate of Ar gas mainly consists of nanoparticles along with very few ultrathin nanowires. At the same temperature (850 °C), if the flow rate of the Ar gas was increased, the percentage of the nanowires increased to a considerable amount (Figure 1b). Figure 1c shows the formation of a large quantity of ultralong ZnS nanowires at 950 °C and a lower Ar flow rate. The diameter of these nanowires varied within 15–25 nm, and their lengths varied within a few tens to a hundred micrometers. A change of morphology was observed at this particular temperature by increasing the flow rate of the Ar gas. In this case, instead of the nanowires, nanoribbons with a width within 20–40 nm were formed in some patches (Figure 1d), whereas a thick layer of long nanoribbons (Figure 1e) was produced at 1050 °C with a lower Ar flow rate. The width of these nanoribbons was found to lie within 100–200 nm, and their lengths varied within a few tens to a hundred micrometers. When the flow rate of the Ar gas was increased to 1050 °C, instead of the uniform layer, nanoribbons with larger width (up to micrometer order) were found in some patches (Figure 1f). On the other hand, at 1150 °C and a lower Ar flow rate, nanoribbons having a width  $\sim 1 \mu\text{m}$  were observed along with some clusters of micro



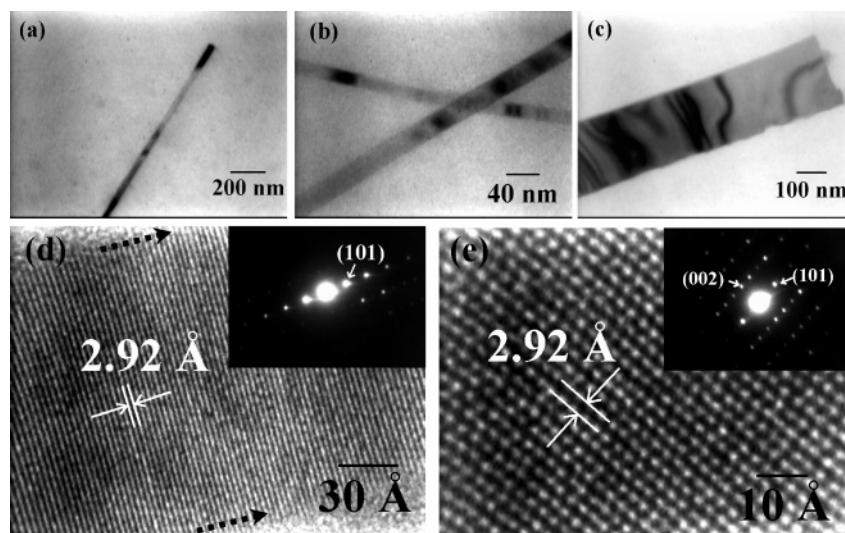
**Figure 2.** (a) XRD pattern of the as-deposited ZnS nanowires revealing the wurtzite phase and (b) EDAX spectrum taken from the ZnS nanowires.

particles having a diameter above a hundred nanometers (Figure 1g). At this temperature (1150 °C), with an increased Ar flow rate, only microcrystals (Figure 1h) were obtained over the Si substrates and no nanoribbons were observed.

**Structural and Compositional Analysis.** XRD patterns of all of the samples, except those produced at 850 °C, were almost identical. Figure 2a shows the XRD spectra of the nanowires with all of the peaks representing the hexagonal wurtzite phase of ZnS with the lattice constants  $a = 3.82 \text{ \AA}$  and  $c = 6.25 \text{ \AA}$ , which matches well with those in the JCPDS (Joint Committee on Powder Diffraction Standards, card no. 36-1450). The XRD patterns of the samples produced at 850 °C (not shown here) were also due to the wurtzite ZnS, but their peaks were broadened due to the presence of the large number of nanoparticles. The chemical composition and the stoichiometry of the ZnS nanostructures were investigated through EDAX. Figure 2b shows the EDAX spectra of the nanowires produced at 950 °C, revealing the chemical purity of the ZnS nanowires. Similar observations were noticed from the EDAX spectrum recorded for all other samples, except the samples corresponding to Figure 1a, b, and d. The EDAX spectra from these samples (not shown here) reveal the presence of Si and a very weak signal due to Au along with those of Zn and S. The Si peak originated from the uncovered Si wafer and Au signal arising from the catalyst used to promote the one-dimensional growth. Elemental analysis reveals the atomic percentages of Zn and S to be 51.6 and 48.4, respectively, which is consistent with the stoichiometric ZnS within the experimental error.

The structure and morphology of the ZnS nanostructures were further studied by the TEM. Figure 3a, b, and c shows the bright field TEM images of ZnS nanowire and nanoribbons. The ripple-like contrasts observed in the ZnS nanowire and nanoribbon were due to the strain resulting from the bending. Figure 3d shows the HRTEM image of a single nanowire having a diameter of  $\sim 15 \text{ nm}$ . The HRTEM image reveals the perfect hexagonal wurtzite  $-2H$  structure of ZnS with a  $[101]$  zone axis, while the corresponding selected area electron diffraction (SAED) taken perpendicular to the axis of the nanowire is shown in the inset of Figure 3c. The measured spacing of the crystallographic planes is  $2.92 \text{ \AA}$ , as shown in Figure 3c, which corresponds to the  $\{101\}$  lattice fringes of the wurtzite ZnS,

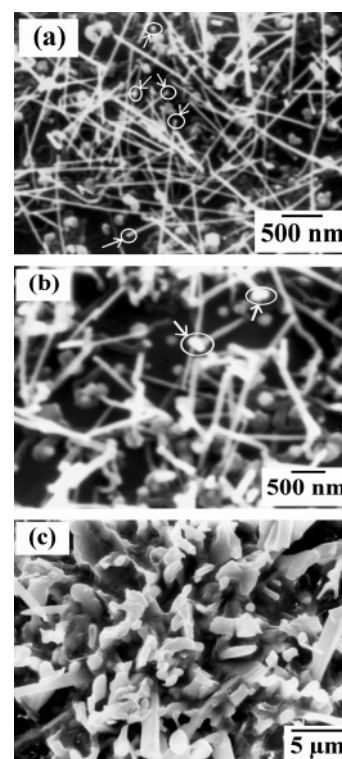




**Figure 3.** TEM images: (a) a single nanowire, (b) two nanoribbons with a width within 20–30 nm, and (c) a nanoribbon with a larger width. The HRTEM images: (d) a single nanowire and (e) a single nanoribbon along with their SAED patterns in the corresponding insets. The arrow in Figure 3d indicates the boundary and growth direction of the nanowire.

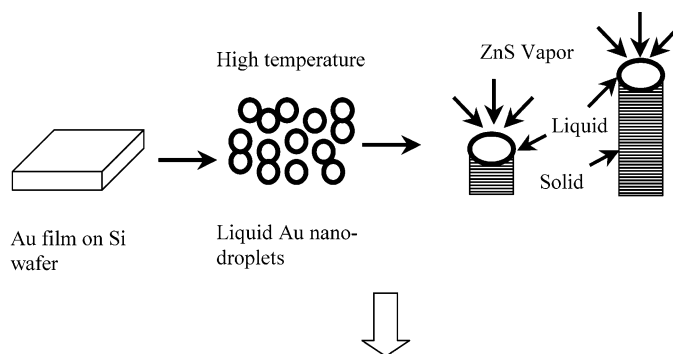
and this is the growth direction of the nanowire. The HRTEM image along with the SAED pattern in the inset taken from a single ZnS nanoribbon is shown in Figure 3d. The measured spacing of the crystallographic planes is also 2.92 Å for the nanoribbons, which corresponds to the {101} planes of the wurtzite ZnS and coincides with the growth direction. The HRTEM image and SAED pattern taken from several nanowires and nanoribbons reveal the formation of dislocation-free single-crystalline ZnS nanostructures.

**Growth Mechanism.** The growth mechanism can be well understood on the basis of the vapor–liquid–solid (VLS) technique.<sup>21</sup> The Au film at high-temperature broke up, and liquid Au nanodroplets were formed on the Si surface. These liquid Au droplets at high temperature absorbed ZnS vapor, and Au–ZnS nanocomposite alloy particles were formed. On supersaturation, pure ZnS nanostructures were originated from these composite particles. Depending on the experimental parameters such as temperature and flow rate of the Ar gas, these liquid composite particles took different shapes, and different morphologies of the ZnS nanostructures originated from them. To investigate the reason behind the morphological change of ZnS nanostructures with the experimental parameters, all of the synthesis procedures corresponding to Figure 1 were repeated for 15 min only. Figure 4a, b, and c shows the early stages of the nanostructure formation corresponding to the structure shown in Figure 1c, e, and g, respectively. Figure 4a shows the intermediate stage of the nanowire growth, indicating short nanowires with spherical catalyst particles at their tip along with few nanoparticles. With time, these nanowires grew in length. On the other hand, Figure 4b shows the early stage of the nanoribbon growth at 1050 °C, revealing the presence of small cylindrical particles at the tip of the small nanoribbons which give it a hammer-like look. These particles are marked in the picture by an ellipse surrounding it and an arrow pointing toward it. The early stage of the nanostructures corresponding to Figure 1g is shown in Figure 4c. On the basis of these observations, we propose a growth scheme shown in Scheme 1. We believe that not only the temperature, but also the concentration of the ZnS vapor and the flow rate of the Ar gas are crucial in defining the morphology of the ZnS nanostructures. The initial ZnS vapor concentration surrounding the Au droplets on the Si substrates is dependent on the temperature. On the other hand, as the substrates were mounted parallel to




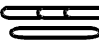

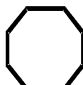


**Figure 4.** SEM images showing the early stage of the growth of ZnS nanostructures: (a) nanorods, (b) short nanoribbons with hammerlike structure, and (c) a mixture of micro particles and short ribbons. The arrow and ellipse drawn in (a) and (b) indicate the presence and shape of the catalyst nanoparticles at the tip of the nanostructures.

the Ar flow path, the flow rate played a crucial role in determining the initial shape of the Au droplets. So, at 850 °C, due to the lack of ZnS vapor concentration surrounding the Au droplets, the absorption and precipitation processes were rather slow, resulting in the formation of nanoparticles along with a few thin nanowires. At an enhanced Ar flow rate, the amount of ZnS vapor flowing across the Si wafer is increased, resulting in the increase in the percentage of the nanowires. At 950 °C with lower Ar flow rate, the ZnS vapor surrounding the spherical Au droplets was sufficient enough to promote the nanowire growth. With the increase in temperature and flow rate, the shape of these Au droplets changed to elliptical, and two or more Au

**SCHEME 1: Proposed Schematic Representation of the Growth Mechanism**

At different deposition condition Au nano-droplets took different shapes resulting in the

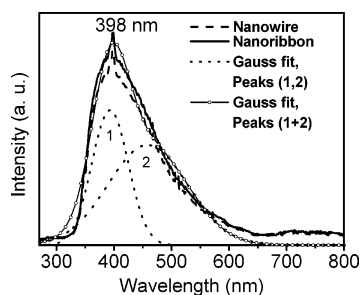
Temperature	950 °C		1050 °C		1150 °C	
Ar flow rate	Low	High	Low	High	Low	High
Initial shape of the Au/ZnS composite alloy droplets						
Resulting Nanostructure	Nano-wire	Nano-ribbon	Nano-ribbon	Nano-ribbon	Nanoribbon & microparticles	Microcrystals
Supporting Figures	Figs. 1c & 4a	Fig. 1e	Figs. 1d & 4b	Fig. 1f	Figs. 1g & 4c	Fig. 1h

formation of different ZnS nanostructures.

Low: 100 cc / min. and High: 800 cc / min.

droplets might have merged to give some cylindrical particles. These cylindrical Au droplets cause the nanoribbon growth as already revealed by Figure 4b. Because of their large surface area, these cylindrical Au droplets absorbed ZnS vapor quickly, resulting in the formation of very long nanoribbons. At 1150 °C and a lower Ar flow rate, the Au droplets might have gathered at several points with some spherical as well as a few cylindrical droplets which were the origin of the microstructures shown in Figure 1g. These assemblies might have merged together due to the agitation caused by the higher Ar flow rate, giving rise to the ZnS microstructures corresponding to Figure 1h.

The placement of the substrates close to the ZnS source enhanced the absorption of ZnS vapor by Au droplets followed by quick precipitation of solid ZnS from the composite droplets resulting in the rapid growth of the ZnS nanostructures. The small agitation caused by the Ar flow might have also enhanced the precipitation of ZnS from the Au–ZnS composite liquid droplets.



**Figure 5.** The photoluminescence spectra taken from the ZnS nanowires and nanoribbons at room temperature with 250 nm excitation.

**Photoluminescence Property.** The photoluminescence (PL) measurement of the ZnS nanostructures was carried out at room temperature with 250 nm excitation. PL spectra taken from both the nanowires and the nanoribbons show almost identical nature. Figure 5 shows strong and broad emission spectra from both the nanowires and the nanoribbons, which are mainly located in the blue region with its maximum intensity centered at ~398 nm. Multipeak Gaussian fitting gives two Gaussian bands located at 394 and 458 nm, respectively. It is shown that the Gaussian curve fits well with the experimental curve. Therefore, the PL spectra of the ZnS nanostructures mainly consist of two bands at 394 and 456 nm. Hu et al.<sup>22</sup> have reported emissions from ZnS nanobelts at 400 nm, and they have attributed this peak to the sulfur vacancy and interstitial lattice defects in the ZnS nanobelts, whereas the emission band at around 450 nm is associated with the trapped luminescence arising from the surface states.<sup>23–25</sup>

### Conclusions

In conclusion, rapid large-scale production of wurtzite ZnS nanowires and nanoribbons has been achieved by thermal evaporation of ZnS powder onto Si substrate in the presence of Au catalyst. Morphologies of the ZnS nanostructures were controlled by varying the temperature, as well as the flow rate of the Ar gas. ZnS nanoribbons were obtained even at 950 °C by increasing the Ar flow rate. Both nanowires and nanoribbons showed almost identical blue luminescence at room temperature.

**Acknowledgment.** We would like to express our sincere gratitude to Mr. K. K. Das of IACS, Kolkata, for recording the SEM images. We are also grateful to DST, Government of India, for financial assistance during the tenure of the program (Nanophase-III).

## References and Notes

- (1) Sooklal, K.; Cullum, B. S.; Angel, S. M.; Murphy, C. J. *J. Phys. Chem.* **1996**, *100*, 4551.
- (2) Falcony, C.; Garcia, M.; Ortiz, A.; Alonso, J. C. *J. Appl. Phys.* **1992**, *72*, 1525.
- (3) Tang, W.; Cameron, D. C. *Thin Solid Films* **1996**, *280*, 221.
- (4) Bredol, M.; Merikhi, J. *J. Mater. Sci.* **1998**, *33*, 471.
- (5) Prevenslik, T. V. *J. Lumin.* **2000**, 87–89, 1210.
- (6) Wada, Y.; Yin, H.; Kitamura, T.; Yanagida, S. *Chem. Commun.* **1998**, *24*, 2683.
- (7) Fujiwara, H.; Hosokawa, H.; Murakoshi, K.; Wada, Y.; Yanagida, S. *Langmuir* **1998**, *14*, 5154.
- (8) Dhas, N. A.; Zaban, A.; Gedanken, A. *Chem. Mater.* **1999**, *11*, 806.
- (9) Frank, S.; Poncharal, P.; Wang, Z. L.; Heer, W. A. *Science* **1998**, *280*, 1744.
- (10) Heath, J. R.; Kuekes, P. J.; Snider, G. S.; Williams, R. S. *Science* **1998**, *280*, 1716.
- (11) Hu, J.; Ouyang, M.; Yang, P.; Lieber, C. M. *Nature* **1999**, *399*, 48.
- (12) Xu, D.; Guo, G.; Gui, L.; Tang, Y.; Shi, Z.; Jin, Z.; Gu, Z.; Liu, W.; Li, X.; Zhang, G. *Appl. Phys. Lett.* **1999**, *75*, 481.
- (13) Chen, X.; Xu, H.; Xu, N.; Zhao, F.; Lin, W.; Lin, G.; Fu, Y.; Huang, Z.; Wang, H.; Wu, M. *Inorg. Chem.* **2003**, *42*, 3100.
- (14) Wang, Y.; Zhang, L.; Liang, C.; Wang, G.; Peng, X. *Chem. Phys. Lett.* **2002**, *357*, 314.
- (15) Meng, X. M.; Liu, J.; Jiang, Y.; Chen, W. W.; Lee, C. S.; Bello, I.; Lee, S. T. *Chem. Phys. Lett.* **2003**, *382*, 434.
- (16) Li, Q.; Wang, C. *Appl. Phys. Lett.* **2003**, *83*, 359.
- (17) Zhu, Y. C.; Bando, Y.; Xue, D. F. *Appl. Phys. Lett.* **2003**, *82*, 1769.
- (18) Jiang, Y.; Meng, X. M.; Liu, J.; Xie, Z. Y.; Lee, C. S.; Lee, S. T. *Adv. Mater.* **2003**, *15*, 323.
- (19) Wang, X.; Gao, P.; Li, J.; Summers, C. J.; Wang, Z. L. *Adv. Mater.* **2002**, *14*, 1732.
- (20) Jiang, X.; Xie, Y.; Lu, J.; Zhu, L.; He, W.; Qian, Y. *Chem. Mater.* **2001**, *13*, 1213.
- (21) Wu, Y.; Yang, P. *J. Am. Chem. Soc.* **2001**, *123*, 3165.
- (22) Hu, P.; Liu, Y.; Fu, L.; Cao, L.; Zhu, D. *J. Phys. Chem. B* **2004**, *108*, 936.
- (23) Denzler, D.; Olschewski, M.; Sattler, K. *J. Appl. Phys.* **1998**, *84*, 2841.
- (24) Bol, A. A.; Meijerink, A. *Phys. Rev. B* **1998**, *58*, R15997.
- (25) Yang, P.; Lu, M.; Xu, D.; Yuan, D. L.; Zhou, G. J. *Chem. Phys. Lett.* **2001**, *336*, 76.